Thermodynamic Characterization of Allosteric Glycogen Phosphorylase Inhibitors

Oliver Anderka,* Petra Loenze, Thomas Klabunde, Matthias K. Dreyer, Elisabeth Defossa, K. Ulrich Wendt, and Dieter Schmoll

Research and Development, Sanofi Aventis Deutschland GmbH, D-65926 Frankfurt am Main, Germany

Received December 7, 2007; Revised Manuscript Received February 26, 2008

ABSTRACT: Glycogen phosphorylase (GP) is a validated target for the treatment of type 2 diabetes. Here we describe highly potent GP inhibitors, AVE5688, AVE2865, and AVE9423. The first two compounds are optimized members of the acyl urea series. The latter represents a novel quinolone class of GP inhibitors, which is introduced in this study. In the enzyme assay, both inhibitor types compete with the physiological activator AMP and act synergistically with glucose. Isothermal titration calorimetry (ITC) shows that the compounds strongly bind to nonphosphorylated, inactive GP (GPb). Binding to phosphorylated, active GP (GPa) is substantially weaker, and the thermodynamic profile reflects a coupled transition to the inactive (tense) conformation. Crystal structures confirm that the three inhibitors bind to the AMP site of tense state GP. These data provide the first direct evidence that acyl urea and quinolone compounds are allosteric inhibitors that selectively bind to and stabilize the inactive conformation of the enzyme. Furthermore, ITC reveals markedly different thermodynamic contributions to inhibitor potency that can be related to the binding modes observed in the cocrystal structures. For AVE5688, which occupies only the lower part of the bifurcated AMP site, binding to GPb (K_d = 170 nM) is exclusively enthalpic ($\Delta H = -9.0$ kcal/mol, $T\Delta S = 0.3$ kcal/mol). The inhibitors AVE2865 (K_d = 9 nM, $\Delta H = -6.8$ kcal/mol, $T\Delta S = 4.2$ kcal/mol) and AVE9423 (K_d = 24 nM, $\Delta H = -5.9$ kcal/mol, $T\Delta S = 4.6$ kcal/mol) fully exploit the volume of the binding pocket. Their pronounced binding entropy can be attributed to the extensive displacement of solvent molecules as well as to ionic interactions with the phosphate recognition site.

Type 2 diabetes is associated with elevated blood glucose levels that in part result from increased hepatic glucose production (*1, 2*). Gluconeogenesis and glycogenolysis, the pathways by which glucose is formed in the liver, are therefore potential targets for pharmacological treatment of this disease. Glycogen phosphorylase (GP) catalyzes the rate-limiting step of glycogen breakdown, the phosphorolytic cleavage of the α-1,4-linked glycosyl units, to yield glucose 1-phosphate. In recent years, several potent inhibitors of GP (GPIs)[1] have been developed. These compounds decrease blood glucose levels in vivo and thereby validate GP as a target for the treatment of diabetes (*3*). Interestingly, GP inhibitors have also been shown to impair the growth of some cancer cells in vitro, suggesting an antioncogenic potential (*4–6*).

Three isozymes of GP with a high degree of sequence homology have been described, hepatic, muscle, and brain forms. GP is regulated by both reversible phosphorylation and allosteric effectors (*7*). According to the Monod−Wyman−Changeux model for allosteric enzymes, homodimeric GP exists in two forms, the active relaxed (R) state and the less active tense (T) state. Phosphorylation of GP leading to GPa promotes the R state. This conformation is also induced by AMP, which acts as an allosteric activator, especially of the muscle isoform. Dephosphorylation of GPa leading to GPb, as well as inhibitors such as glucose, favors the T state.

So far, GP inhibitors have been identified which bind to either the active site, the binding site of the allosteric effector AMP (AMP site), the purine site, or the indole site (*3*). Recently, acyl ureas were described as a novel class of phosphorylase inhibitors (*8*). As shown by X-ray crystallography, these compounds bind to the AMP site of GP (*9*). In the study presented here, we report two optimized members of the acyl urea series (AVE5688 and AVE2865). With the quinolone compound AVE9423, a novel chemical class of GPIs is introduced here. AVE9423 and AVE2865 are among the most potent GP inhibitors reported so far (*3*). We apply enzyme kinetics, isothermal titration calorimetry (ITC), and protein crystallography in analyzing and comparing the binding mode of these compounds. This combined approach clearly demonstrates that these compounds are allosteric inhibitors that stabilize the inactive tense state of the enzyme. Furthermore, this study provides insights into the driving forces of inhibitor binding and the principles underlying their efficacy.

* To whom correspondence should be addressed. Telephone: +49-69-305-12418. Fax: +49-69-305-81901. E-mail: oliver.anderka@sanofi-aventis.com.

[1] Abbreviations: ASA, accessible surface area; BES, *N*,*N*-bis(2-hydroxyethyl)-2-aminoethanesulfonic acid; DMSO, dimethyl sulfoxide; GPa and GPb, glycogen phosphorylases a and b, respectively; GPI, glycogen phosphorylase inhibitor; hlGP, human liver glycogen phosphorylase; HEPES, *N*-(2-hydroxyethyl)piperazine-*N*′-(2-ethanesulfonic acid); ITC, isothermal titration calorimetry; MES, 4-morpholineethanesulfonic acid; MPD, 2-methyl-2,4-pentanediol; rmGP, rabbit muscle glycogen phosphorylase; Tris, 2-amino-2-(hydroxymethyl)-1,3-propanediol.

10.1021/bi702397d CCC: $40.75
Published on Web 03/29/2008

EXPERIMENTAL PROCEDURES

Chemical Synthesis. Glycogen phosphorylase inhibitors AVE5688, AVE2865, and AVE9423 were synthesized as described elsewhere (*10–12*).

Enzyme Preparation. Phosphorylated and unphosphorylated rabbit muscle glycogen phosphorylase (rmGPa and rmGPb, respectively) were purchased from Sigma-Aldrich Co. (St. Louis, MO). Human liver glycogen phosphorylase (hlGPa) was purified as described elsewhere (*13*).

Enzymatic Inhibition Assay. Glycogen phosphorylase activity was measured in the physiological direction of glycogen breakdown as previously described (*8*). rmGP was used for the kinetic characterization of the inhibitors. To routinely check the phosphorylation grade of enzyme batches, activity was measured in the direction of glycogen synthesis (*8*); the phosphorylation grade was estimated from the ratio of the activity in the presence of 0.5 mM caffeine to the activity in the presence of 2 mM AMP.

Isothermal Titration Calorimetry. ITC measurements were carried out on a VP-ITC ultrasensitive titration calorimeter (MicroCal Inc., Northampton, MA). rmGP samples were dialyzed twice for several hours at 4 °C against the measuring buffer and centrifuged (20000*g*, 15 min, 4 °C) to remove insoluble matter. The dialysis buffer was used in preparation of all protein and ligand solutions. The enzyme concentration was determined from UV absorbance measurements using a molar extinction coefficient at 280 nm of 128280 M^{-1} (*14*). Unless otherwise stated, the measuring cell contained 10 μM enzyme and the syringe contained 100 μM inhibitor as a titrant; both solutions were in 40 mM Tris-HCl and 0.1 mM β-mercaptoethanol (pH 7.4). The default measuring temperature was 25 °C. The compound solutions were prepared from a 10 mM stock in DMSO; to match the buffer composition, corresponding amounts of the organic solvent (1%) were added to the protein solution. After an initial injection of 5 μL which was not used for data fitting, 19 injections of 15 μL each were performed at 300 s intervals. Blank titrations of inhibitor into buffer were also performed to correct for heats generated by dilution and mixing. The heat evolved after each injection was obtained from the time integral of the calorimetric signal, and data were fit to a binding model using Origin version 7.0 (OriginLab Corp., Northampton, MA).

To correlate the change in buried surface area (ΔASA_{np}, ΔASA_p) to the binding heat capacity (ΔC_p) and enthalpy (ΔH) changes, the following empirical relationships were applied: $\Delta C_p = 0.45\Delta ASA_{np} - 0.26\Delta ASA_p$ and $\Delta H_{60} = -8.44\Delta ASA_{np} + 31.4\Delta ASA_p$, where ΔH_{60} is the extrapolated binding enthalpy change at 60 °C in kilocalories per mole (*15, 16*).

X-ray Crystallography. For cocrystallization, hlGPa was concentrated to 7 mg/mL in a solution containing 20 mM BES (pH 6.5), 1 mM EDTA, and 0.5 mM DTT. After concentration, the glucose analogue β-*N*-acetylglucosamine at 50 mM and the respective inhibitor at 2.5 mM were added. The resulting solution was incubated at 4 °C for 2 h before hanging drops were set up by mixing equal volumes of the protein solution with a reservoir solution containing 30% MPD and 100 mM MES (pH 6.0). Crystal growth, data collection, and structure determination were performed as previously described (*8*). The inhibitors were defined well in the experimental $F_o - F_c$ electron densities that were calculated using Protein Data Bank entry 1FC0 as a starting model (*13*). All structures were refined using standard crystallographic software. The atomic coordinates are deposited in the Protein Data Bank as entries 3CEH (AVE5688), 3CEJ (AVE2865), and 3CEM (AVE9423).

Scheme 1: Chemical Structures of the Acyl Urea Compounds AVE5688 and AVE2865 and the Quinolone AVE9423[a]

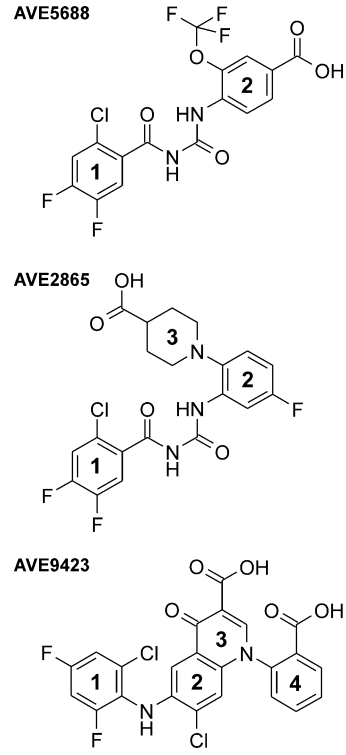

[a] For easier reference, the ring systems are numbered.

RESULTS

Structures of the investigated phosphorylase inhibitors are shown in Scheme 1. AVE5688 and AVE2865 are highly active representatives from the acyl urea series of inhibitors. AVE9423 represents a novel class of GP inhibitors reported in this work which contain a central quinolone moiety.

Kinetic Characterization. The effects of the compounds on GP activity were measured in the direction of glycogenolysis. The IC_{50} values of the GPIs for the inhibition of rmGPa and rmGPb are summarized in Table 1. The GPb preparation contained approximately 10% GPa (data not shown) which will significantly contribute to the detected enzymatic activity. Nevertheless, the observation that the IC_{50} values toward GPb were consistently lower compared to those toward GPa suggests a higher affinity of the inhibitors for the nonphosphorylated enzyme.

Second, kinetic measurements were performed in the presence of AMP, an allosteric activator of the enzyme (Figure 1a). With rmGPb, the IC_{50} values of the compounds increase with an increase in AMP concentration, yet a potent inhibition is observed. However, for rmGPa in the presence of 30 μM AMP, even with the compounds at 10 μM, the enzyme was only weakly inhibited (not shown). Third, IC_{50} values of the inhibitors were determined in the presence of glucose, a negative effector of GPa (Figure 1b). The

Table 1: Enzymatic[a] and Thermodynamic[b] Data for Inhibitor Binding to rmGP

enzyme	compound	IC_{50} (nM)	N^c	K_d (nM)	ΔH (kcal/mol)	$T\Delta S$ (kcal/mol)	$\Delta C_p{}^d$ (cal mol^{-1} K^{-1})
rmGPb	AVE5688	430 ± 36	1.0 ± 0.1	170 ± 49	−9.0 ± 0.4	0.3 ± 0.4	−156 ± 50
	AVE2865	14 ± 1	1.0 ± 0.1	9 ± 2	−6.8 ± 0.3	4.2 ± 0.4	−282 ± 29
	AVE9423	44 ± 6	0.9 ± 0.1	24 ± 12	−5.9 ± 0.3	4.6 ± 0.6	−418 ± 24
rmGPa	AVE5688	915 ± 45	0.8 ± 0.1	530 ± 206	2.1 ± 0.6	10.7 ± 0.8	−430 ± 69
	AVE2865	24 ± 1	1.1 ± 0.1	74 ± 27	8.6 ± 0.8	18.3 ± 0.8	−760± 46
	AVE9423	59 ± 6	1.0 ± 0.0	240 ± 122	9.6 ± 0.2	18.6 ± 0.5	−858 ± 81

[a] IC_{50} values are means ± the standard deviation from four experiments. [b] ITC measurements were performed in triplicate, and values are given as means ± the standard deviation. [c] Stoichiometry of the enzyme–inhibitor complex. [d] The change in heat capacity ΔC_p was obtained from the data shown in Figure 4.

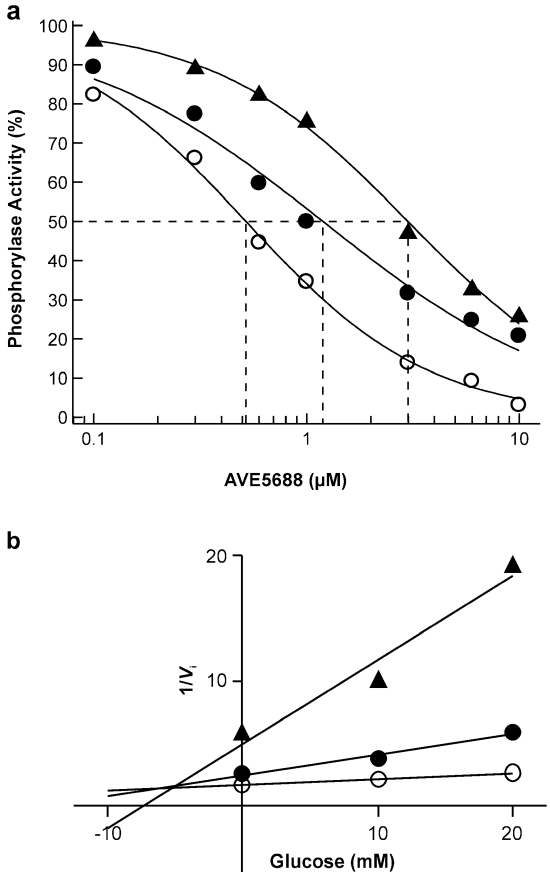

FIGURE 1: Effect of AMP and glucose on inhibition kinetics. Shown are exemplary data. Analogous results were obtained with the other compounds. (a) Inhibition of rmGPb by AVE5688 was assessed in the absence (○) or presence of 30 μM (●) and 1 mM AMP (▲). (b) rmGPa initial reaction rates were measured in the absence or presence of 10 and 20 mM glucose, without (○) or with 30 nM (●) and 100 nM AVE9423 (▲). Dixon plot of reciprocal velocity vs glucose concentration. Symbols represent data from a single experiment performed in duplicate.

intersection of the lines at different glucose concentrations above the *x*-axis of the Dixon plot suggests a synergistic action of glucose and GPIs (*17*). This finding is in line with evidence demonstrating different binding sites for the acyl ureas (AMP site) and glucose (active site) and furthermore suggests that the novel quinolone GPI AVE9423 acts via a similar mechanism.

Isothermal Titration Calorimetry. ITC titrations of the inhibitors with either rmGPa or rmGPb were performed to (i) further investigate the inhibitory mechanism of the GPIs and (ii) establish a detailed analysis of the thermodynamic forces underlying the potency of the three described compounds. Figure 2a shows exemplary raw data from a single experiment. In Figure 2b, the isotherms for binding of the different inhibitors to either rmGPa or rmGPb are overlaid. The thermodynamic data that were obtained from the ITC titrations are given in Table 1. The data clearly establish a 1:1 stoichiometry for the three investigated protein–ligand complexes (based on GP monomeric half-concentration). The order of K_d values reflects the order of inhibitor potency (Table 1). Importantly, the ITC data directly show that the three investigated GPIs bind much more strongly to rmGPb than to rmGPa ($P < 0.01$).

The thermodynamic profiles of binding were completely different for the interaction of the inhibitors with the phosphorylated enzyme (GPa) versus the nonphosphorylated enzyme (GPb). For all three inhibitors, we observed exothermic binding to rmGPb. The weakest inhibitor, AVE5688, shows the largest (i.e., most negative) enthalpic contribution. However, its entropy term of binding ($T\Delta S$) is close to zero, whereas the high-affinity inhibitors AVE2865 and AVE9423 have much larger entropic contributions to the free energy of binding. On the other hand, the binding to the phosphorylated enzyme (rmGPa) is exclusively entropy driven for all three inhibitors, and the lower affinity for the phosphorylated enzyme stems from a positive ΔH term, indicating a significant enthalpic "penalty" of binding.

Effect of Glucose on the Binding Isotherms. α-D-Glucose is a physiological inhibitor of GP activity ($K_i = 2$ mM). It binds to the catalytic site and shifts the conformational equilibrium of GPa toward the inactive T state (*18*). We examined the effect of glucose on the binding of the inhibitors by ITC. Whereas binding of GPI to rmGPb is unchanged by the presence of 10 mM glucose (not shown), the binding isotherm for rmGPa is strongly affected [Figure 3 (▲); data shown for AVE9423, comparable observations made for AVE5688 and AVE2865]. The curve becomes biphasic with an exothermic high-affinity phase ($N_1 = 0.4$, $K_{d1} = 15$ nM, $\Delta H_1 = -1.3$ kcal/mol) that resembles the rmGPb binding isotherm, and an endothermic lower-affinity component ($N_2 = 0.6$, $K_{d2} = 82$ nM, $\Delta H_2 = 6.8$ kcal/mol), similar to that seen for rmGPa in the absence of glucose [Figure 3 (△)]. This glucose effect supports the notion that the GPIs bind selectively to the inactive T state with high affinity and in an exothermic manner. Preincubation of GPa with glucose increases the population of the T state in solution.

Heat Capacity Changes upon Binding. The change in heat capacity ($\Delta C_p = d\Delta H/dT$) is sensitive to the extent of hydration of molecular surfaces (*19, 20*). To determine the ΔC_p of binding, ITC titrations of rmGPa and rmGPb with the three inhibitors were performed over a range of temperatures, and the obtained ΔH values were plotted against temperature (Figure 4). A linear change of ΔH with

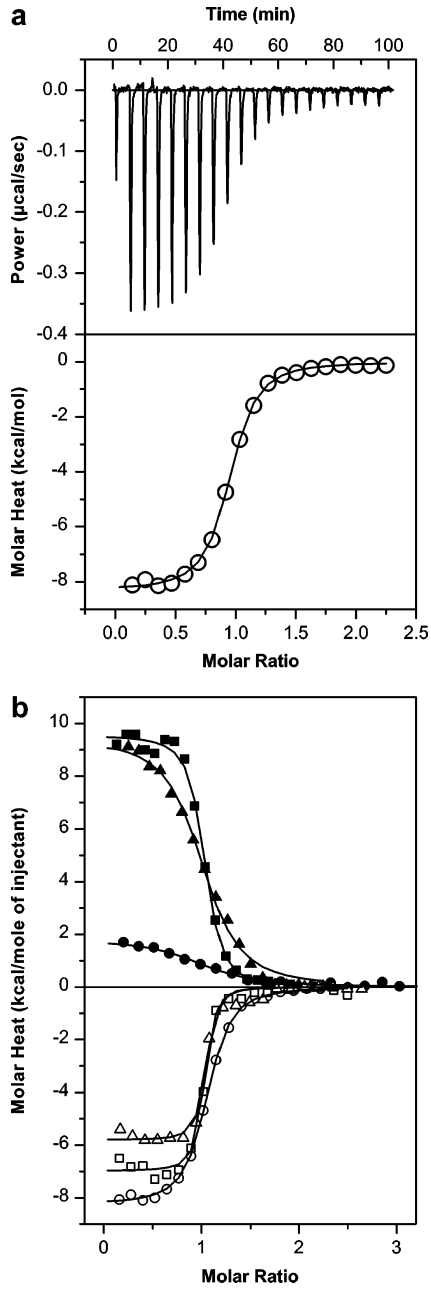

FIGURE 2: Exemplary data from ITC experiments. (a) Sample titration of rmGPb with AVE5688. Shown in the top panel are raw heating power data; the first peak represents a smaller preinjection (5 μL) that is omitted in the integrated data. Shown in the bottom panel are data after peak integration, subtraction of blank titration data (not shown), and concentration normalization. Molar heats of binding are plotted vs the molar ratio of titrant to protein. The solid line is the fit to a single-site binding model. (b) Normalized and integrated heat data for titrations of rmGPa (filled symbols) or rmGPb (empty symbols) with AVE5688 (circles), AVE2865 (squares), and AVE9423 (triangles). The solid lines represent fits to a single-site binding model.

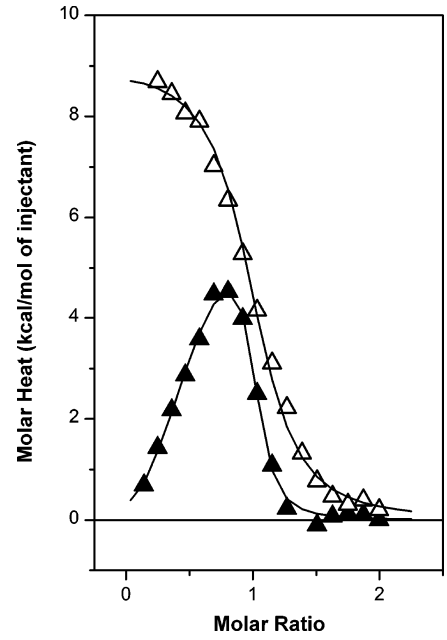

FIGURE 3: Effect of glucose on binding of AVE9423 to rmGPa. Measurements were performed in the presence (▲) or absence (△) of 10 mM glucose in both cell and syringe solutions. Normalized and integrated heat data were fit to a two-site (with glucose) or one-site (without glucose) binding model.

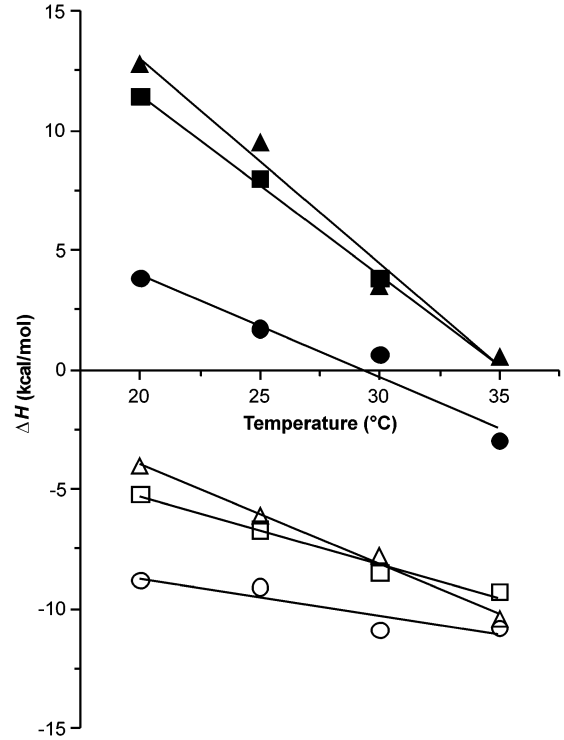

FIGURE 4: Temperature dependence of binding enthalpy. Enthalpy values from titrations of rmGPa (filled symbols) or rmGPb (empty symbols) with AVE5688 (circles), AVE2865 (squares), and AVE9423 (triangles). The pH was adjusted for each temperature to account for the relatively strong temperature dependence of Tris buffer. Each data point represents the average enthalpy value from one to three independent ITC titrations. The slope of the temperature dependence of ΔH provides the ΔC_p of binding.

temperature was observed, and ΔC_p values were obtained from the slope of the regression curve (Table 1). It was found that the lower-affinity compound AVE5688 produced a smaller change in heat capacity than AVE2865 and AVE9423. The ΔC_p values were considerably larger (approximately twice) for inhibitor binding to rmGPa compared to GPb. This observed large heat capacity change upon binding to rmGPa could be caused by the conformational change that is coupled to binding (see the Discussion). To test this hypothesis, we applied equations that correlate ΔC_p and ΔH values to the change in accessible surface area (ΔASA) upon binding (*15, 21*). In agreement with our assumption, the ΔASA (as calculated from the cocrystal structures; see below) is

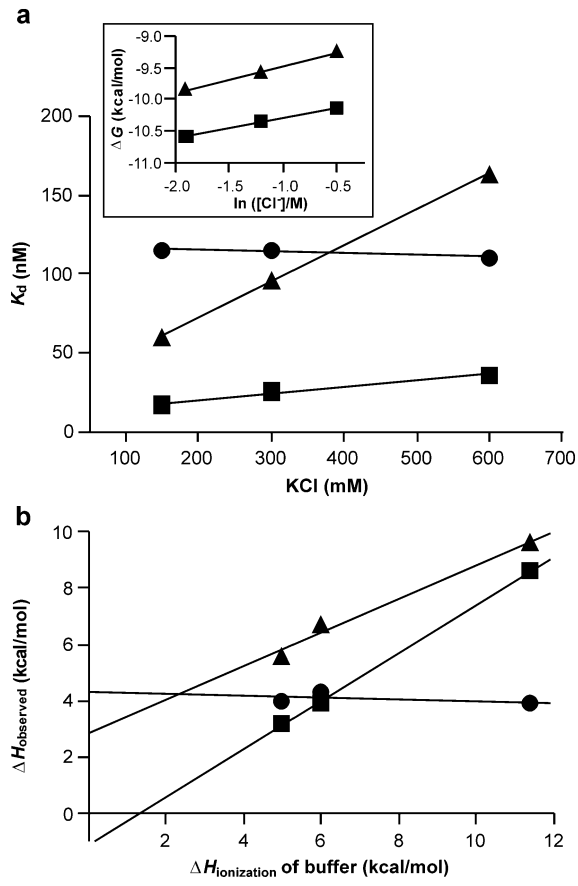

FIGURE 5: Salt and buffer effects. (a) Dependence of binding affinity on salt concentration. ITC titrations of rmGPb with AVE5688 (●), AVE2865 (■), and AVE9423 (▲) were performed at different salt concentrations. Each data point represents the K_d value obtained from an ITC titration. The inset shows a plot of ΔG vs ln[Cl^-] from the experiments with AVE2865 (■) and AVE9423 (▲). (b) Dependence of apparent binding enthalpy on the buffer deprotonation enthalpy. Titrations of rmGPa with AVE5688 (●), AVE2865 (■), and AVE9423 (▲) were performed at 25 °C in 40 mM Tris, 50 mM BES, or 80 mM HEPES, 0.1 mM β-mercaptoethanol, and 1% DMSO (pH 7.4). Different concentrations of the buffer substances were used to match the ionic strength. ΔH_{obs} was obtained from a single-binding site fit of the ITC isotherms. Each data point represents the average enthalpy value from at least two independent ITC titrations. Values for ΔH_{ion} were obtained from the literature (*24, 26*). The sign and magnitude of the slope of ΔH_{obs} vs ΔH_{ion} provide the direction (here, from the buffer to the inhibitor−enzyme complex) and average number of protons transferred.

severalfold overestimated on the basis of the thermodynamic parameters (data not shown).

Effect of Buffer Conditions. As all three inhibitors, as well as the allosteric binding site, have ionizable groups, we examined the effect of salt concentration on compound affinity toward GPb (Figure 5a). AVE5688 binding is independent of ionic strength. For the other two compounds, binding becomes weaker when the salt concentration is increased. The salt effect is more pronounced for AVE9423 (slope of K_d vs salt concentration of 0.23) than for AVE2865 (slope of 0.04). Assuming a simple competitive model, the number of counterions that are displaced by the ligand can be calculated according to the equation $\partial\Delta G/\partial(\ln[Cl^-]) = RT\langle i\rangle$, where $\langle i\rangle$ is the mean number of ions released upon binding (*22*). The slope of ΔG versus ln[Cl^-] (inset of Figure 5a) leads to values of 0.5 (AVE2865) and 0.7 (AVE9423) for $\langle i\rangle$, which predicts the release of approximately one counterion upon compound binding to the allosteric AMP pocket.

The binding interaction may also involve the transfer of protons to or from the complex. With ITC, proton transfer can be determined by measuring the observed ΔH of binding in buffers with different enthalpies of deprotonation (*23, 24*): $\Delta H_{obs} = \Delta H_{int} + n\Delta H_{ion}$, where ΔH_{int} is the intrinsic heat of binding, independent of buffer protonation effects, and the magnitude and sign of n give the net number of protons transferred during binding and the direction of transfer, respectively. Titrations were carried out in three different buffers. For rmGPb, no buffer dependency of ΔH was observed (data not shown). Also with AVE5688 binding to rmGPa, there was no buffer effect (Figure 5b; slope of –0.04 ± 0.05), which indicates that no net proton transfer occurred upon binding of this compound. However, for rmGPa together with the high-affinity inhibitors AVE2865 and AVE9423, the observed binding enthalpy changed linearly as the ΔH_{ion} of the buffer was varied. The slopes of the linear regression were 0.85 ± 0.02 (AVE2865) and 0.60 ± 0.07 (AVE9423). This means that for AVE2865 and AVE9423, a net average of about one proton is transferred to the enzyme−GPI complex during binding to rmGPa at neutral or slightly alkaline pH. The assignment of the protonation event to a specific residue is not possible in the absence of further information, e.g., from site-directed mutations.

The determination of ΔC_p values (Table 1) was performed in Tris buffer, which has a relatively large enthalpy of deprotonation that contributes to the measured heats of AVE2865 and AVE9423 binding to GPa. The enthalpy of Tris deprotonation is also temperature-dependent (ΔC_p = –11.9 cal mol^{-1} K^{-1}) (*25*), which introduces an error of 1–2% into the observed ΔC_p values of compound binding. We regard this error as negligible.

Structural Characterization. To complement the kinetic and thermodynamic data, the inhibitors were cocrystallized with hlGPa in the presence of a glucose analogue and the X-ray structures were determined (Table 2). In line with the kinetic characterization, both the acyl urea compounds and the novel GPI AVE9423 were found to bind (i) to the allosteric AMP site of the enzyme (ii) in a conformation that resembles the tense state of the enzyme (Figure 6). All three inhibitors bind in a position that partially overlaps with the position of AMP as observed within the hlGP−AMP complex (PDB entry 1FA9) (*13*). The binding position of the three inhibitors is not compatible with the enzyme conformation seen in the relaxed state. The allosteric site is located at the dimer interface of the enzyme; in the following, residues from the symmetry-related subunit are denoted with a prime. For ease of discussion, the AMP site can be divided into a "lower" and an "upper" half.

As in previous structures from this series (*8, 9*), the less potent inhibitor AVE5688 binds only to the lower subsite. The acyl urea moiety of this ligand forms hydrogen bonds with the backbone of Val40′ and Asp42′, thereby stabilizing the enzyme in its tense state conformation. In addition, the acyl urea forms a hydrogen bond to an ordered water molecule in the upper part of the binding pocket. The halogenated benzoyl ring is buried in a narrow side pocket in the lower part of the AMP site. It shows cation−π stacking with Arg193, a $\pi-\pi$ stacking interaction with the side chain

Table 2: Summary of Diffraction Data and Refinement Statistics for hlGPa in Complex with AVE5688, AVE2865, and AVE9423

	hlGPa−AVE5688	hlGPa−AVE2865	hlGPa−AVE9423
	Data Processing		
resolution (Å) (last shell)	2.80 (2.87–2.80)	3.30 (3.38–3.30)	2.47 (2.53–2.47)
space group	144	144	144
cell dimensions *a*, *b*, *c* (Å)	124.1, 124.1, 122.5	123.3, 123.3, 121.9	124.4, 124.4, 123.4
cell dimensions α, *β*, *γ* (deg)	90, 90, 120	90, 90, 120	90, 90, 120
total no. of reflections	93921	67989	263008
no. of unique reflections	51525	25212	76587
R_{sym} (%)	10.8 (40.9)	13.3 (39.7)	8.1 (37.1)
completeness (%)	99.2 (99.0)	80.8 (82.8)	99.9 (100.0)
mean I/σ	6.1 (1.9)	7.3 (2.9)	11.6 (3.5)
	Refinement		
R_{cryst} (%)	16.9 (24.4)	18.0 (22.7)	15.9 (21.4)
R_{free} (%)	24.7 (32.8)	27.0 (35.4)	21.1 (28.7)
root-mean-square deviation for bonds (Å)	0.014	0.009	0.020
root-mean-square deviation for angles (deg)	1.559	1.259	1.845
no. of protein atoms	12938	12834	12939
no. of solvent atoms	508	141	500
no. of ligand atoms	142	124	130

of Trp67, and a hydrophobic interaction with Val40′. The phenyl ring (ring 2 in Scheme 1) on the other hand points toward the exit of the binding site. It shows van der Waals contacts with Gln72, Tyr75, and Val45′; its trifluoromethoxy substituent hydrophobically interacts with Tyr75.

AVE2865 is a highly potent acyl urea GPI. The interactions of AVE2865 in the lower AMP site are very similar to the binding pattern of AVE5688. In addition, AVE2865 interacts with the upper AMP site, where the carboxylate group of the 4-carboxyl-piperidine substituent forms a salt bridge to Arg309 and Arg310. Both arginines are located in a cluster of basic residues which are involved in the binding of the phosphate moiety of the physiological ligand AMP. In the AVE2865 crystal structure, ordered solvent molecules were not found in the upper binding site. Accordingly, no water-mediated hydrogen bond of the acyl urea was observed. However, this finding is tentative due to the moderate resolution of the AVE2865 crystal structure (3.3 Å).

The binding pattern of AVE9423, a representative of the novel quinolone series, generally compares well to that of the acyl urea AVE2865. Like the halogen-substituted benzoyl ring of the acyl urea series, the halogenated phenyl ring of the quinolone (ring 1 in Scheme 1) binds within a deep side pocket where it forms similar interactions (cation−π to Arg193, $\pi-\pi$ stacking with Trp67, and hydrophobic interaction with Val40′). The chlorine substituent at the quinolone shows hydrophobic interactions with the aliphatic side chains of Ile68 and Val45′. Stacking with Tyr75 can be observed for the benzoic acid ring (ring 4 in Scheme 1) at the AMP site entrance. Like AVE2865, AVE9423 fills the upper AMP site. Here, the resolution is sufficient (2.5 Å) to ascertain that (ordered) water molecules are excluded from this volume. The ionic interactions with the arginine cluster are even more pronounced compared to those with AVE2865 due to the delocalized negative charge (contact to Arg193, Arg242, Arg309, and Arg310).

For the change in accessible surface area (ΔASA) upon binding of the inhibitors, the following values were determined (which refer to the sum of enzyme and GPI surface area): 560 Å^2 for AVE5688, 670 Å^2 for AVE2865, and 670 Å^2 for AVE9423.

DISCUSSION

Mechanism of Inhibition. The kinetic data (Figure 1) show that the inhibitors (i) are antagonized by the physiological activator AMP and (ii) act in a synergistic fashion with the negative effector glucose. Most importantly, the ITC experiments reveal that the inhibitors bind to nonphosphorylated, predominantly inactive (tense) rmGPb with an affinity ∼1 order of magnitude higher than that for phosphorylated, active (relaxed) rmGPa (Table 1). Furthermore, glucose shifts the binding behavior for GPa to "GPb-like", whereas binding to GPb remains unchanged (Figure 3). The thermodynamic binding data provide the first direct evidence that acyl urea and quinolone inhibitors stabilize the inactive tense conformation (T state) of the enzyme, in line with the Monod−Wyman−Changeux model for the regulation of allosteric enzymes.

Our crystal structures show that compounds AVE5688, AVE2865, and AVE9423 bind to the allosteric AMP site of human liver phosphorylase (Figure 6). This has been described before for acyl ureas (*9*) but is also found for AVE9423, a member of the novel quinolone class of GPIs (this study). The position of the inhibitors in the allosteric site is distinct but overlapping with the position that AMP would adopt. Therefore, binding of AMP and GPI is mutually exclusive. As already reported for previous compounds from this series (*9*), also acyl ureas AVE5688 and AVE2865 cocrystallize with the tense state of the enzyme. The same observation can be made for the novel quinolone AVE9423. Modeled superposition of the compounds with the active state enzyme results in steric clashes. This further supports the conclusion from the calorimetric data that the GPIs selectively bind to the inactive tense state GP.

The ITC experiments show that binding of the inhibitors to GPa versus GPb is characterized not only by different affinities but also by a strikingly different thermodynamic pattern (Table 1). We conclude that the thermodynamic values observed with GPb represent "intrinsic" inhibitor binding, whereas the values obtained with GPa also include the relaxed-to-tense state conformational transition of the enzyme, which is a prerequisite for binding. On the basis of the observed values (Table 1), we conclude that the R → T

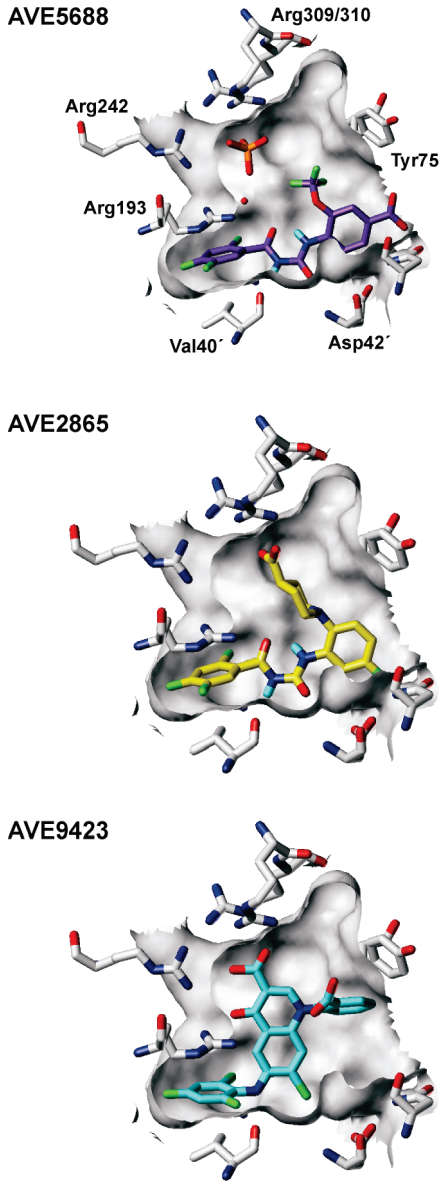

FIGURE 6: Binding mode of the inhibitors AVE5688, AVE2865, and AVE9423 at the allosteric AMP site of hlGPa. The structure of the bound GPI is shown as a stick model for the three inhibitors in purple, yellow, and cyan, respectively. Only polar hydrogens of the inhibitor molecules are shown. Amino acid residues relevant for binding are shown as stick models. For clarity, the solvent accessible surface of the binding pocket is shown. The upper AMP pocket in the AVE5688 structure contains an ordered water molecule (red) and a phosphate ion.

transition of GP is entropy-driven and enthalpically disfavored. This is consistent with previous crystallographic analyses which suggested that the transition to the inactive state leads to (i) reduced solvent accessibility of a central cavity between the GP subunits (entropy gain) (*27*) and (ii) a net loss of hydrogen bonds (enthalpy cost) (*28*). Further support comes from thermodynamic investigations of AMP binding to GPb (*29*), which induces a T → R transition. This process is enthalpy-driven and entropically costly and therefore represents a "mirror image" of GPI binding to GPa. The major conformational transition between the relaxed and tense state of GP is also reflected in the changes in heat capacity ΔC_p (Figure 4). The unusually negative ΔC_p values observed for GPa (Table 1) are indicative of coupled conformational changes (*21, 30*). Taken together, the thermodynamic features confirm that for inhibitor binding GPa has to adopt the tense state.

A potential flaw in this study is that for reasons of limited protein availability the human liver enzyme (hlGP) was used for crystallography whereas the kinetic and thermodynamic characterization was performed with rabbit muscle phosphorylase (rmGP). However, for the following reasons, we think that it is valid to directly compare the obtained data. (i) The two isoforms are highly similar (*31*). (ii) Both enzyme variants are inhibited by acyl urea compounds with similar potencies (*8, 9*). (iii) The acyl ureas bind in a superimposable way to both isoforms (*8, 9*). In fact, 19 of the 20 amino acids that are in the first shell around the AMP site of rmGP and hlGP are identical. The only difference is an Asp−Glu exchange, and this residue is not involved in contacts with the inhibitor.

Thermodynamics Underlying Inhibitor Potency. ITC analysis of binding processes complements structural information as it reveals the underlying contributions of enthalpy and entropy. Considering that very high affinity can only be achieved if both ΔH and ΔS contribute favorably to the binding free energy, ITC analysis can give valuable information for the optimization of lead compounds during drug development (*32*). From a thermodynamic perspective, enthalpy-driven binders are the preferred starting points for lead optimization (*33*).

This principle is exemplified by the moderate-affinity acyl urea AVE5688 (K_d = 170 nM for rmGPb), which was subsequently optimized toward the highly potent AVE2865 (K_d = 9 nM). Thermodynamic values are discussed in the following with respect to the GPI−rmGPb interaction (intrinsic binding; see above). AVE5688 is a strongly enthalpy driven binder (Table 1), which indicates a predominantly polar interaction. This is confirmed by the cocrystal structure which shows that AVE5688 forms several hydrogen bonds within the binding pocket. However, the affinity of AVE5688 is not yet optimal due to the poor binding entropy of the compound. A major entropic contribution to binding affinity comes from the release of water into the bulk solvent (*34*). In the AVE5688 complex structure, solvent molecules were still observed in the upper part of the binding pocket. At least one of them is involved in mediating specific bonds from the inhibitor to the enzyme (Figure 6). This observation can provide a structural explanation for the small entropy gain of AVE5688 binding.

In contrast to AVE5688, the high-affinity compound AVE2865 extends into the upper pocket of the allosteric site (Figure 6), probably leading to a more complete exclusion of solvent. Furthermore, the compound likely forms salt bridges with the arginine cluster of the phosphate recognition site. An ionic contribution is confirmed by the salt dependence of the binding affinity (Figure 5a). Ionic interactions are often entropically favorable, while not having a large effect on ΔH (*35*). Taken together, both solvent exclusion and charge–charge interactions explain the superior binding entropy of AVE2865 compared to AVE5688.

Binding thermodynamics of AVE9423 as a representative of the novel quinolone class of GP inhibitors closely resemble the values observed for the acyl urea AVE2865. A similar binding mode of the two compounds would therefore be anticipated from the ITC data. This is confirmed by the cocrystal structure. Like AVE2865, the quinolone compound

AVE9423 also extends into the upper part of the AMP site, which displaces solvent molecules. Similar observations were made for another potent AMP site inhibitor, BAY W1807 (*36*). These findings stress the importance of solvent molecules in inhibitor design, in a manner independent of the chemical structure. Due to a partially delocalized negative charge, the salt bridge network of AVE9423 with the arginine cluster of the phosphate recognition site is even more extensive than for AVE2865. In agreement with the structural observation, the salt dependence for AVE9423 binding is more pronounced than for AVE2865 (Figure 5a). A larger ionic contribution is in line with the slightly superior entropy of the quinolone compound relative to the acyl urea.

This study demonstrates that ITC measurements provide a thermodynamic fingerprint of drug–protein interactions, which can be related to the molecular mode of binding. Calorimetric data can therefore be useful to complement X-ray crystallography. However, even in the absence of structural information, thermodynamics can give a guideline to improve drug potency. Comparisons of drug binding energetics and structure are still rather scarce in the literature (*37*). Therefore, every case study will contribute to the understanding of structure−thermodynamics relationships.

ACKNOWLEDGMENT

We thank Michael Bauer, Peter-Michael Blohm, Nicole Hoerl, Dieter Kadereit, Wolfgang Roehner, Detlev Schneider, Karl Schoenafinger, and Herbert Weber for the chemical synthesis of the described compounds. Furthermore, we thank Anke Müller-Seeland for assistance in kinetic measurements and Volker Brachvogel for the support in protein crystallography.

REFERENCES

1. Lefebvre, P. J., and Scheen, A. J. (1999) Glucose metabolism and the postprandial state. *Eur. J. Clin. Invest. 29* (Suppl. 2), 1–6.
2. Roden, M., and Bernroider, E. (2003) Hepatic glucose metabolism in humans: Its role in health and disease. *Best Pract. Res., Clin. Endocrinol. Metab. 17*, 365–383.
3. Henke, B. R., and Sparks, S. M. (2006) Glycogen phosphorylase inhibitors. *Mini-Rev. Med. Chem. 6*, 845–857.
4. Lee, W. N., Guo, P., Lim, S., Bassilian, S., Lee, S. T., Boren, J., Cascante, M., Go, V. L., and Boros, L. G. (2004) Metabolic sensitivity of pancreatic tumour cell apoptosis to glycogen phosphorylase inhibitor treatment. *Br. J. Cancer 91*, 2094–2100.
5. Schnier, J. B., Nishi, K., Monks, A., Gorin, F. A., and Bradbury, E. M. (2003) Inhibition of glycogen phosphorylase (GP) by CP-91,149 induces growth inhibition correlating with brain GP expression. *Biochem. Biophys. Res. Commun. 309*, 126–134.
6. Schnier, J. B., Nishi, K., Gumerlock, P. H., Gorin, F. A., and Bradbury, E. M. (2005) Glycogen synthesis correlates with androgen-dependent growth arrest in prostate cancer. *BMC Urol. 5*, 6.
7. Johnson, L. N. (1992) Glycogen phosphorylase: Control by phosphorylation and allosteric effectors. *FASEB J. 6*, 2274–2282.
8. Klabunde, T., Wendt, K. U., Kadereit, D., Brachvogel, V., Burger, H. J., Herling, A. W., Oikonomakos, N. G., Kosmopoulou, M. N., Schmoll, D., Sarubbi, E., von Roedern, E., Schoenafinger, K., and Defossa, E. (2005) Acyl ureas as human liver glycogen phosphorylase inhibitors for the treatment of type 2 diabetes. *J. Med. Chem. 48*, 6178–6193.
9. Oikonomakos, N. G., Kosmopoulou, M. N., Chrysina, E. D., Leonidas, D. D., Kostas, I. D., Wendt, K. U., Klabunde, T., and Defossa, E. (2005) Crystallographic studies on acyl ureas, a new class of glycogen phosphorylase inhibitors, as potential antidiabetic drugs. *Protein Sci. 14*, 1760–1771.
10. Defossa, E., Kadereit, D., Schoenafinger, K., Klabunde, T., Burger, H. J., Herling, A. W., Wendt, K. U., von Roedern, E., Ehnsen, A., and Rieke-Zapp, J. (2003) Preparation of 4-(benzoylureido)-benzoic acids as antidiabetics. WO2003084922, example 49.
11. Schoenafinger, K., Defossa, E., Kadereit, D., von Roedern, E., Klabunde, T., Burger, H. J., Herling, A. W., and Wendt, K. U. (2004) Preparation of heterocyclylbenzoylureas for treating type 2 diabetes. WO2004007455, example 16.
12. Defossa, E., Kadereit, D., Ruf, S., Klabunde, T., Schmoll, D., Herling, A. W., and Wendt, K. U. (2005) 7-Phenylamino-4-quinolone-3-carboxylic acid derivatives, methods for production and use thereof as medicaments. WO2005073229, example 325.
13. Rath, V. L., Ammirati, M., LeMotte, P. K., Fennell, K. F., Mansour, M. N., Danley, D. E., Hynes, T. R., Schulte, G. K., Wasilko, D. J., and Pandit, J. (2000) Activation of human liver glycogen phosphorylase by alteration of the secondary structure and packing of the catalytic core. *Mol. Cell 6*, 139–148.
14. Kastenschmidt, L. L., Kastenschmidt, J., and Helmreich, E. (1968) Subunit interactions and their relationship to the allosteric properties of rabbit skeletal muscle phosphorylase b. *Biochemistry 7*, 3590–3608.
15. Murphy, K. P., and Freire, E. (1992) Thermodynamics of structural stability and cooperative folding behavior in proteins. *Adv. Protein Chem. 43*, 313–361.
16. Xie, D., and Freire, E. (1994) Molecular basis of cooperativity in protein folding. V. Thermodynamic and structural conditions for the stabilization of compact denatured states. *Proteins 19*, 291–301.
17. Segel, I. H. (1993) *Enzyme Kinetics*, Wiley, New York.
18. Sprang, S. R., Goldsmith, E. J., Fletterick, R. J., Withers, S. G., and Madsen, N. B. (1982) Catalytic site of glycogen phosphorylase: Structure of the T state and specificity for α-D-glucose. *Biochemistry 21*, 5364–5371.
19. Spolar, R. S., Livingstone, J. R., and Record, M. T., Jr. (1992) Use of liquid hydrocarbon and amide transfer data to estimate contributions to thermodynamic functions of protein folding from the removal of nonpolar and polar surface from water. *Biochemistry 31*, 3947–3955.
20. Gomez, J., Hilser, V. J., Xie, D., and Freire, E. (1995) The heat capacity of proteins. *Proteins 22*, 404–412.
21. Spolar, R. S., and Record, M. T., Jr. (1994) Coupling of local folding to site-specific binding of proteins to DNA. *Science 263*, 777–784.
22. Guzman-Casado, M., Sanchez-Ruiz, J. M., El, H. M., Gimenez-Gallego, G., and Parody-Morreale, A. (2000) Energetics of myo-inositol hexasulfate binding to human acidic fibroblast growth factor effect of ionic strength and temperature. *Eur. J. Biochem. 267*, 3477–3486.
23. Murphy, K. P., Xie, D., Garcia, K. C., Amzel, L. M., and Freire, E. (1993) Structural energetics of peptide recognition: Angiotensin II/antibody binding. *Proteins 15*, 113–120.
24. Fukada, H., and Takahashi, K. (1998) Enthalpy and heat capacity changes for the proton dissociation of various buffer components in 0.1 M potassium chloride. *Proteins 33*, 159–166.
25. Bates, R. G., and Hetzer, H. B. (1961) Dissociation constant of the protonated acid form of 2-amino-2-(hydroxymethyl)-1,3-propanediol [tris(hydroxymethyl)-aminomethane] and related thermodynamic quantities from 0 to 50°. *J. Phys. Chem. 65*, 667–671.
26. Thomson, J. A., and Ladbury, J. E. (2004) Isothermal Titration Calorimetry: A Tutorial, in *Biocalorimetry 2* (Ladbury, J. E., and Doyle, M. L., Eds.) 1st ed., pp 37–58, John Wiley & Sons Ltd., Chichester, England.
27. Sprang, S., and Fletterick, R. J. (1980) Subunit interactions and the allosteric response in phosphorylase. *Biophys. J. 32*, 175–192.
28. Buchbinder, J. L., Rath, V. L., and Fletterick, R. J. (2001) Structural relationships among regulated and unregulated phosphorylases. *Annu. Rev. Biophys. Biomol. Struct. 30*, 191–209.
29. Baron, C., Gonzalez, J. F., Mateo, P. L., and Cortijo, M. (1989) Thermodynamic analysis of the activation of glycogen phosphorylase b over a range of temperatures. *J. Biol. Chem. 264*, 12872–12878.
30. Leder, L., Berger, C., Bornhauser, S., Wendt, H., Ackermann, F., Jelesarov, I., and Bosshard, H. R. (1995) Spectroscopic, calorimetric, and kinetic demonstration of conformational adaptation in peptide-antibody recognition. *Biochemistry 34*, 16509–16518.
31. Rath, V. L., Newgard, C. B., Sprang, S. R., Goldsmith, E. J., and Fletterick, R. J. (1987) Modeling the biochemical differences between rabbit muscle and human liver phosphorylase. *Proteins 2*, 225–235.
32. Holdgate, G. A., and Ward, W. H. (2005) Measurements of binding thermodynamics in drug discovery. *Drug Discovery Today 10*, 1543–1550.

33. Velazquez, C. A., and Freire, E. (2005) ITC in the post-genomic era. .? Priceless. *Biophys. Chem. 115*, 115–124.
34. Ward, W. H., and Holdgate, G. A. (2001) Isothermal titration calorimetry in drug discovery. *Prog. Med. Chem. 38*, 309–376.
35. Holdgate, G. A. (2001) Making cool drugs hot: Isothermal titration calorimetry as a tool to study binding energetics. *BioTechniques 31*, 164–184.
36. Oikonomakos, N. G., Tsitsanou, K. E., Zographos, S. E., Skamnaki, V. T., Goldmann, S., and Bischoff, H. (1999) Allosteric inhibition of glycogen phosphorylase a by the potential antidiabetic drug 3-isopropyl 4-(2-chlorophenyl)-1,4-dihydro-1-ethyl-2-methyl-pyridine-3,5,6-tricarboxylate. *Protein Sci. 8*, 1930–1945.
37. Steuber, H., Heine, A., and Klebe, G. (2007) Structural and thermodynamic study on aldose reductase: Nitro-substituted inhibitors with strong enthalpic binding contribution. *J. Mol. Biol. 368*, 618–638.

BI702397D